Annals of Nuclear Energy 211 (2025) 110950

Contents lists available at ScienceDirect

Annals of Nuclear Energy

journal homepage: www.elsevier.com/locate/anucene

Fuel performance modelling of Cr-coated Zircaloy cladding under DBA/LOCA conditions

Pau Aragón [a,b,*], Francisco Feria [a,*], Luis E. Herranz [a], Arndt Schubert [c], Paul Van Uffelen [c]

[a] CIEMAT, Unit of Nuclear Safety Research, Av. Complutense, 40, 28040 Madrid, Spain
[b] Universidad Politécnica de Madrid (UPM), Energy Engineering Department, José Gutiérrez Abascal, 2, 28006 Madrid, Spain
[c] European Commission, Joint Research Centre (JRC), Karlsruhe, Germany

ARTICLE INFO

Keywords:
Fuel safety
Fuel performance modelling
LOCA
FRAPTRAN
TRANSURANUS
ATF
Coating

ABSTRACT

Chromium coatings are being developed for advanced technology fuel (ATF) claddings, offering negligible corrosion during normal operation, improved resistance to high-temperature steam oxidation, and superior high-temperature strength, the latter two being of utmost relevance during design basis accidents (DBAs). Demonstrating the improved response of Cr-coated Zircaloy requires the development or extension of fuel performance codes to coating simulations.

In this work, material models and correlations for Cr-coated Zircaloy cladding have been derived or obtained from the literature and implemented into TRANSURANUS and the FRAPTRAN-TUmech suite. These extended tools have been used to simulate two complementary LOCA tests: QUENCH-L1 rod 4 (out-of-pile bundle test on fresh Zircaloy cladding) and IFA-650.10 (in-pile single rod test on high-burnup Zircaloy-UO_2 fuel), enabling a gradual cross-verification of results between codes and a comparative performance analysis between coated and uncoated cladding.

The results indicate negligible impact of coating properties other than creep on the burst time. While the superior high-temperature creep resistance of coated cladding slightly delays the burst time, additional burst data would be necessary to draw sound conclusions on the balloon size. Regarding the modelling approach, treating the coated cladding as a composite material through the definition of effective properties might result in worse performance relative to uncoated cladding, contradicting experimental observations. Therefore, the separate modelling of the coating and the cladding is recommended.

1. Introduction

Metallic chromium-based coatings are currently under development for advanced technology fuel (ATF) cladding applications. While these coatings constitute only a small fraction of the total cladding thickness, their design aims to offer minimal corrosion during normal operation and to enhance high-temperature strength and steam oxidation kinetics under accident scenarios. The massive production of hydrogen during the Fukushima-Daiichi accident fostered investigations into assessing the behaviour of coated claddings under loss-of-coolant accidents (LOCAs) (NEA, 2018). For that purpose, the predictive capabilities of existing fuel performance codes must be updated.

Fuel performance modelling studies in the open literature have primarily focused on steady-state conditions (Lee et al., 2017; Ševeček et al., 2018), LOCA (Dunbar et al., 2024; Lee et al., 2023a; Ma et al., 2021; Sweet et al., 2022), and short-term station blackout events (Guo et al., 2021) conditions. Additionally, Wagih et al. (2018) conducted fuel performance simulations under steady-state, power ramp, and LOCA scenarios. Notably, all comparative analyses of coated and uncoated cladding under LOCA conditions utilized the BISON or ABAQUS finite-element codes, as well as the MARS-KS system code. Moreover, none of these analyses included simulations of high burnup fuel, except for a recent study by Dunbar et al. (2024).

To further demonstrate the potential benefits of coated cladding over uncoated cladding under LOCA conditions, conducting fuel performance simulations across a representative range of burnups becomes imperative. As the nuclear industry currently explores the possibility of increasing the burnup limit (e.g., beyond 62 MWd/kgU rod-average burnup for all U.S. nuclear fuel vendors), addressing this need is equally critical for high burnup fuel. On the other hand, regarding the

* Corresponding authors at: CIEMAT, Unit of Nuclear Safety Research, Av. Complutense, 40, 28040 Madrid, Spain.
E-mail addresses: pau.aragon@ciemat.es (P. Aragón), francisco.feria@ciemat.es (F. Feria).

https://doi.org/10.1016/j.anucene.2024.110950
Received 12 March 2024; Received in revised form 19 September 2024; Accepted 24 September 2024
Available online 3 October 2024

approach to modelling coated cladding (i.e., separately modelling the coating from the cladding versus treating the coated cladding as a composite material by considering effective properties), there has been a lack of comprehensive discussion on the advantages and drawbacks of each approach based on simulation outcomes. Instead, previous studies have tended to adopt a singular approach (i.e., the multilayer approach) without delving into comparative assessments. Therefore, the impact of the chosen modelling approach on the simulation outcomes remains to be evaluated.

In this work, the fuel performance code TRANSURANUS and the FRAPTRAN-TUmech suite have been extended to simulate Cr-coated Zircaloy cladding. FRAPTRAN-TUmech is the result of coupling a simplified version of the mechanical model in TRANSURANUS with FRAPTRAN-2.0, as outlined in Aragón et al. (2024). These extended tools have been applied to simulate two LOCA tests: QUENCH-L1 rod 4 (out-of-pile fresh Zircaloy cladding bundle test) and IFA-650.10 (in-pile single-rod high-burnup Zircaloy-UO_2 test), enabling a gradual cross-verification of results between codes and a comparative performance analysis between coated and uncoated cladding. The implementation of coatings into TRANSURANUS and FRAPTRAN-TUmech has been conducted according to a review of the material models and correlations available in the open literature, along with the outcomes of two sensitivity analyses. These analyses aimed to determine the impact of failure criteria on burst time and cladding post-burst strains, as well as the differences resulting from the selection of the modelling approach.

2. Material models and correlations

This section provides a review of material models and correlations pertaining to Cr-coated Zr-based claddings found in the open literature. Their range of applicability and associated uncertainty are outlined whenever available. The scope of the review includes models and correlations that characterize the pure coating material (i.e., Cr) as well as effective correlations that treat the coated cladding as a composite material. The thermo-mechanical properties under consideration are thermal conductivity, specific heat, emissivity, thermal expansion, Young's modulus, Poisson's ratio, irradiation swelling and creep, thermal creep, and corrosion. These properties were selected due to their relevance in fuel performance analyses under normal operating conditions and accident scenarios (Geelhood and Luscher, 2019), with no influence from specific code requirements. Additionally, this section presents a compilation of burst data from open literature sources. The impact of the coating technique on the above properties has not been assessed in detail due to the overall lack of specific data. For comparative purposes, the correlations included in TRANSURANUS for a generic Zircaloy cladding (European Commission, 2023) are plotted along with the coating and/or coated cladding data.

Before delving into the details of the aforementioned properties, it is important to highlight that despite the melting temperature of pure Cr being approximately 1863 °C (Holzwarth and Stamm, 2002), an eutectic reaction between Zr and Cr occurs at a temperature close to 1332 °C (Brachet et al., 2020; Yang et al., 2022). The impact of having an eutectic liquid at the outer surface of the cladding on its performance, albeit at temperatures higher than those of DBA conditions, has been studied by several authors. Notably, the effect of eutectic formation on high-temperature steam oxidation was summarized in Brachet et al. (2020).

Regarding the density of pure Cr, it was measured at around 7200 kg/m^3 at room temperature (Simmons and Wang, 1971), which is 10 % higher than that of Zircaloy (6550 kg/m^3). Most of the measurements on pure Cr reported below were conducted by Holzwarth and Stamm (2002). In particular, the examined material was the commercially available Ducropur (99.7 wt% of Cr), produced by Metallwerke Plansee AG.

2.1. Thermal conductivity

The thermal conductivity of Ducropur as a function of temperature was reported in Holzwarth and Stamm (2002). The correlation is applicable between 20 and 1000 °C.

$$\lambda\left[\mathrm{Wm^{-1}K^{-1}}\right] = 87.56671 - 0.04179T + 3.15147\cdot10^{-5}T^2 - 2.06676\cdot10^{-8}T^3 \quad (1)$$

where T is the temperature in °C.

The thermal conductivity of Cr is not anticipated to be strongly affected by neutron irradiation, as heat transfer in a metal primarily relies on freely moving electrons, which are not significantly impacted by lattice damage (Geelhood and Luscher, 2019). Fig. 1 shows that the thermal conductivity of Cr lies well above that of Zircaloy at all temperatures. Hence, this high thermal conductivity, coupled with the relatively thin coating layer (between 10 and 20 μm), is not expected to influence the overall heat transfer across the cladding.

The thermal conductivity of the Cr_2O_3 layer formed during high-temperature steam oxidation (refer to Section 2.8) is also taken into account as an additional thermal resistance in series (see Table 2), in a similar way as the thermal conductivity of ZrO_2 when standard Zircaloy oxidises. However, the formation of $ZrCr_2$ at the interface between the substrate and the coating at high temperatures (Brachet et al., 2020; Lee et al., 2023b) is not considered here.

2.2. Specific heat

The specific heat of Ducropur as a function of temperature was reported in Holzwarth and Stamm (2002). The correlation is applicable between 20 and 1000 °C.

$$c_p\left[\mathrm{Jg^{-1}K^{-1}}\right] = 0.48047 + 6.34753\cdot10^{-5}T + 2.34120\cdot10^{-7}T^2 - 1.27824\cdot10^{-10}T^3 \quad (2)$$

where T is the temperature in °C.

In Fig. 2, the main features of Cr relative to Zircaloy are the absence of a phase transition and its considerably higher specific heat up to 800 °C. However, the significantly lower volume fraction of Cr compared to Zircaloy (less than 4 %) is not expected to impact the overall thermal inertia of the cladding.

2.3. Emissivity

In the present study, tabulated data on the emissivity of oxidized Cr from Shackelford and Alexander (2001) have been fitted to a temperature-dependant second-order polynomial, as shown in Fig. 3. The resultant correlation can be expressed as:

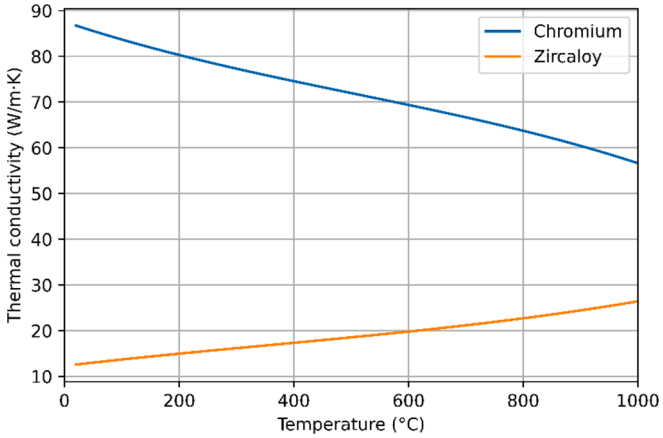

Fig. 1. Thermal conductivity as a function of temperature.

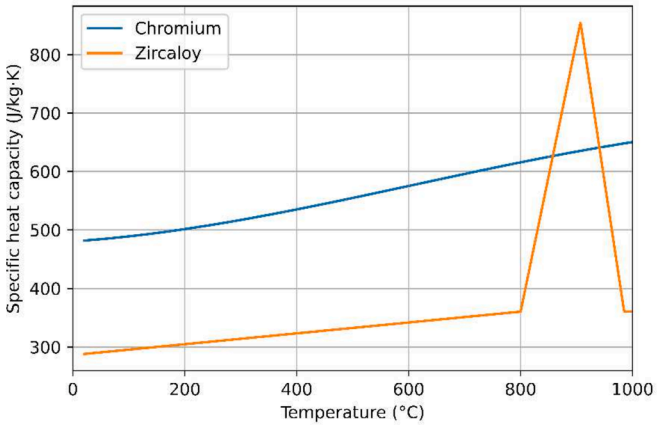

Fig. 2. Specific heat as a function of temperature.

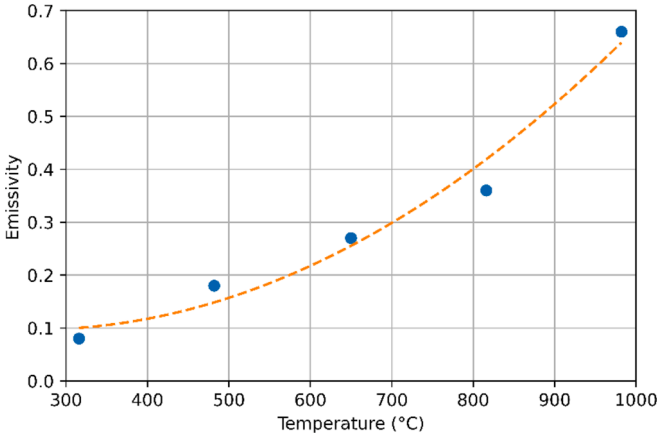

Fig. 3. Emissivity as a function of temperature.

$$\epsilon = 0.167 - 5.40{\cdot}10^{-4}T + 1.04{\cdot}10^{-6}T^2 \tag{3}$$

with the temperature in °C and the coefficient of determination $R^2 = 0.972$.

Within TRANSURANUS, the consideration of cladding emissivity is confined to the gap heat transfer calculation. Since the addition of a coating on the outer surface of the cladding does not entail any change in that regard, Fig. 3 does not include a comparison. Nevertheless, certain severe accident codes account for radiative heat transfer from the cladding outer surface to other core components. Therefore, characterizing the emissivity of the coating becomes relevant in scenarios where such codes are applied.

2.4. Thermal expansion coefficient

The thermal expansion of a material is typically described through its thermal expansion coefficient. In the case of Ducropur, this coefficient was reported in Holzwarth and Stamm (2002) as a function of temperature in °C, as shown in Eq. (4). The correlation applies to pure Cr between 20 and 1000 °C and is depicted in Fig. 4.

$$\alpha\left[\mathrm{K}^{-1}\right] = \left(8.3159 + 1.80901{\cdot}10^{-3}T + 6.45421{\cdot}10^{-7}T^2 + 1.27483{\cdot}10^{-10}T^3\right){\cdot}10^{-6} \tag{4}$$

A potential source of permanent deformation in the coating arises from the differential thermal expansion between the cladding and the coating, the latter being relatively weaker due to its lower thickness. The term 'differential' not only refers to the magnitude of the deviation in their thermal expansion coefficients but also to the direction along which dimensional changes occur. The hexagonal close-packed (HCP) crystal structure of Zircaloy results in anisotropic thermal expansion, while the body-centered cubic (BCC) structure of Cr expands isotropically. It should be noted, however, that the anisotropy of Zircaloy is not accounted for in the correlation shown in Fig. 4. The effect of the thermal expansion mismatch will depend on the tolerance of fabrication methods (i.e., coating deposition techniques) to withstand large strains at the interface between the coating and the cladding.

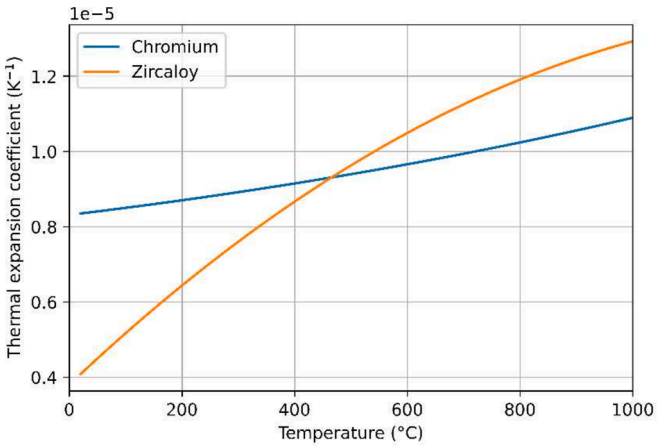

Fig. 4. Thermal expansion coefficient as a function of temperature.

2.5. Elastic constants

Young's modulus of pure Cr as a function of temperature in Kelvin was derived from Armstrong Harry (1964) by Wagih et al. (2018) and Ma et al. (2021). Both correlations are plotted in Fig. 5 and are applicable between 100 and 1250 °C. For simplicity, and given their degree of coherence, only the correlation derived by Wagih et al. is explicitly stated below.

$$E[\mathrm{GPa}] = 264.11 - 0.01T - 2.5{\cdot}10^{-5}T^2 \tag{5}$$

Coated cladding testing conducted by Westinghouse revealed a 25 % increase in (effective) Young's modulus compared to uncoated material (Frederick, 2023). However, the temperature range for this increase was not provided.

As for the Poisson's ratio, a value of 0.22 was measured by Simmons and Wang (1971) at room temperature. No additional data have been found in the open literature. In TRANSURANUS, the Poisson's ratio for a generic Zircaloy cladding is set constant at 0.325 below its melting

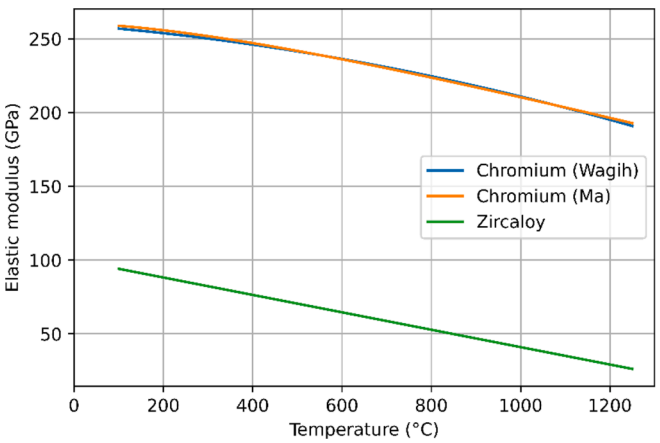

Fig. 5. Young's modulus as a function of temperature.

temperature.

2.6. Irradiation swelling and creep

While the contribution from irradiation swelling and creep to cladding deformation is negligible during short transients, their characterization under reactor conditions is essential to accurately predict the dimensions of the fuel rod at the onset of the transient.

Irradiation creep stands out as the primary mechanism driving the creepdown of the cladding during normal operation conditions as a result of the pressure differential between the coolant and the internal gas. Recent irradiation creep measurements on CrN-coated Zircaloy samples have shown minimal differences from uncoated Zircaloy (Mulligan et al., 2024). Despite the coating material differing from pure Cr, and in the absence of additional data, the irradiation creep models derived for uncoated Zircaloy are recommended for Cr-coated Zircaloy as well.

Irradiation swelling is not observable in anisotropic materials like Zircaloy, which undergoes irradiation growth along the axial direction (Adamson et al., 2017). However, BCC metals such as Cr may experience swelling under irradiation. The post-transient (steady-state) swelling rate of pure Cr was measured at 0.05 % per displacements-per-atom (dpa). Nonetheless, swelling in Cr appears to initiate at a higher rate at very low doses. The lowest experimental data point indicates 0.8 % swelling at 5.9 dpa, suggesting an average swelling rate of 0.14 % per dpa in the 0.0–5.9 dpa range (Gabriel et al., 2022). Therefore, the current authors propose the following model as a first-order approximation to modelling the volumetric swelling strain experienced by pure Cr under irradiation:

$$\varepsilon_s[\%] = 0.14 \cdot \text{dose [dpa]} \text{ if dose} \leq 5.9 \text{ dpa}$$

$$\varepsilon_s[\%] = 0.05 \cdot \text{dose [dpa]} + 0.531 \text{ if dose} > 5.9 \text{ dpa} \quad (6)$$

The linear strain due to irradiation swelling may be calculated as one-third of the volumetric strain based on the small-strain approximation.

Under normal operation conditions, the structural integrity of the coating layer is anticipated to be significantly challenged towards high burnup due to increasing strain mismatch in irradiation-induced axial growth and/or creep (Lee et al., 2017).

2.7. Thermal creep

Ševeček et al. (2018) and Wagih et al. (2018) used data from Stephens and Klopp (1972) to derive a creep correlation for pure Cr in the form of a Norton law:

$$\dot{\varepsilon}_{th} = A\sigma^n \exp(-Q/RT) \quad (7)$$

where $\dot{\varepsilon}_{th}$ is the thermal creep strain rate, σ is the applied stress, R is the universal gas constant, and T is the absolute temperature. A, n, and Q are model parameters.

On the other hand, Ridley et al. (2023b) derived two effective Norton creep laws from coated cladding specimens. Isobaric burst testing with a 5 °C/s heating rate was conducted to determine the activation energy, while isothermal burst testing with multiple pressure steps was performed to calculate the stress exponent. The strength coefficient (A), stress exponent (n), and activation energy (Q) for each correlation are detailed in Table 1. It is important to note that the strength coefficients reported by Ridley et al. are solely for circumferential and not effective strain.

Table 1
Norton creep law parameters.

Material	Procedure	A[MPa^{-n}s^{-1}]	n	Q[kJ/mol]	Reference
Pure Cr	Not specified	5.1596e-3	6.2	306.2688	Wagih et al. (2018)
Cr-coated Zry-4	Isobaric	124 ± 45	6.12	287 ± 22	Ridley et al. (2023b)
Cr-coated Zry-4	Isothermal	43 ± 14	6.12 ± 0.79	287	Ridley et al. (2023b)

Fig. 6 highlights the superior thermal creep resistance of pure Cr compared to Zircaloy when subjected to a linear temperature rise of 6 °C/s from 300 °C at 60 MPa. Fig. 7 provides a zoom-in between 80 and 100 s to facilitate the differentiation between the effective correlations derived from coated samples and the TRANSURANUS correlation recommended for generic Zircaloy cladding (European Commission, 2023).

Note that the correlations derived by Ridley et al. evolve in parallel because they use the same stress exponent and activation energy. Conversely, the strength coefficient derived from isothermal test data is three times lower than that obtained from isobaric data. The reasons behind this difference are unknown and, in any case, fall beyond the scope of this paper. Nevertheless, the authors recommend using the correlation derived from isobaric testing for LOCA simulation, as the testing conditions more accurately represent such a scenario. Additionally, the temperature increase rate of 5 °C/s in the experimental setup aligns with the anticipated rate during the heat-up phase of a LOCA.

In contrast to experimental observations (Brachet et al., 2016; Hazan et al., 2021; Ridley et al., 2023a; Ševeček et al., 2021; Walters et al., 2021), the calculated creep deformation for coated cladding (isobaric) exceeds that of uncoated cladding up to approximately 860 °C, after which the expected behaviour is observed. This outcome is code-dependent, given that the comparison is drawn with the Zircaloy creep equation included in TRANUSRANUS. However, it highlights a potential source of inconsistent results when implementing effective creep laws for coated claddings into fuel performance codes. Further discussion on this topic is provided in Section 3.1 and 4.3.2.

Other studies based on effective creep modelling have applied a global multiplier, denoted as $g(\delta)$, into the baseline Zircaloy model to characterize the thermal creep strain rate ($\dot{\varepsilon}_{th}$) of Cr-coated Zircaloy as a function of the coating thickness δ (Vidal et al., 2022):

$$\dot{\varepsilon}_{th}^{coat} = g(\delta)\dot{\varepsilon}_{th}^{uncoat} = \left(1 + K_\delta \frac{\delta}{r_0 - r_i}\right)\dot{\varepsilon}_{th}^{uncoat} \quad (8)$$

where r_0 and r_i are the cladding outer and inner radius, respectively. The parameter K_δ has been fitted to experimental data from out-of-pile creep tests on coated cladding samples. However, its specific value has not been disclosed.

Finally, regarding the creep anisotropy coefficients, it is assumed that owing to the BCC crystallographic structure of Cr, Cr coatings exhibit isotropic creep behaviour.

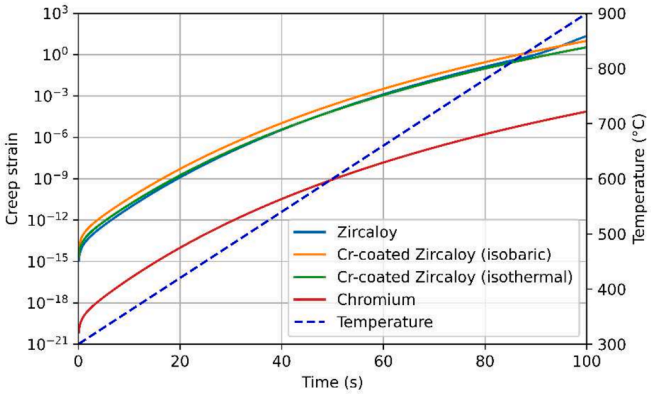

Fig. 6. Thermal creep strain under a linear temperature ramp of 6 °C/s and 60 MPa.

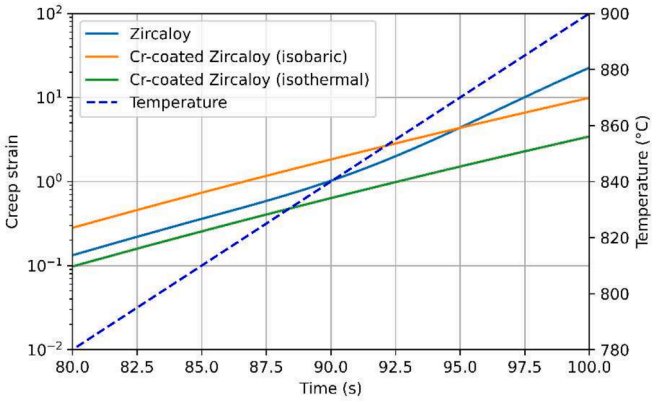

Fig. 7. Zoom-in on Fig. 6 between 80 and 100 s.

2.8. Corrosion

Limited quantitative information has been found on hydrothermal corrosion (i.e., corrosion in high-temperature high-pressure water) and hydrogen pickup of Cr-coated claddings (Bischoff et al., 2016; Brachet et al., 2019; Kim et al., 2015; Lahoda et al., 2018). All these studies indicate that a stable nanometre-size layer of Cr_2O_3 forms under normal operating conditions. Hence, hydrothermal corrosion is negligible under such conditions.

Most available data pertains to high-temperature steam oxidation. The parabolic rate constant describing the high-temperature oxidation of pure Cr as a function of temperature has been extensively measured over several decades. Brachet et al. (2020) conducted a comprehensive literature review, including two recent datasets from CEA and Framatome on Cr-coated Zr-based claddings. These datasets are presented as a function of temperature in Fig. 8 and are fitted to an Arrhenius law with a pre-exponential factor $A = 6.5761 \cdot 10^{-2}$ cm^2/s and activation energy $Q = 238.80$ kJ/mol. The coefficient of determination is $R^2 = 0.966$. Table 2 includes additional parameters describing thermo-physical properties of Cr_2O_3.

Major differences in oxide layer thickness are anticipated between coated and uncoated cladding due to the superior high-temperature steam oxidation resistance of Cr, which leads to orders of magnitude slower reaction rates. In both cases, however, the thermal resistance of the outer oxide layer is accounted for via the thermal conductivity, its higher volume via the Pilling-Bedworth ratio, and the additional heat from the exothermal reaction via the heat of oxidation. What is not yet considered in the current version of the coated cladding corrosion model is the scenario where the entire coating layer is corroded (Lee et al., 2023a).

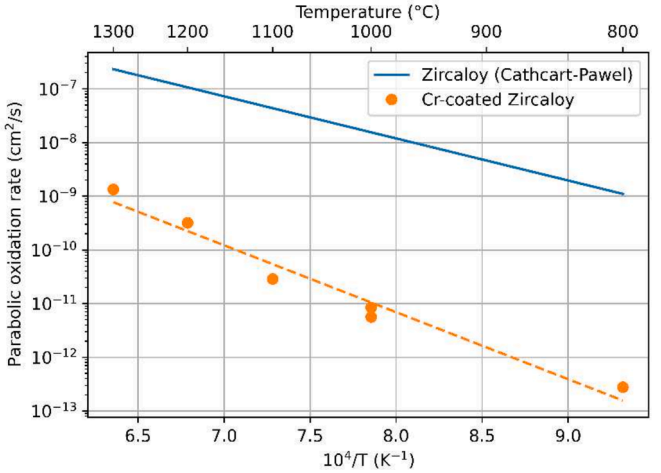

Fig. 8. Parabolic oxidation rate constant as a function of temperature.

Table 2
Thermo-physical properties of chromia.

Chromia parameter	Value	Reference
Density [g/cm^3]	5.21	Shackelford and Alexander (2001)
Heat of oxidation [kJ/mol]	225	Csontos and Capps (2019)
Thermal conductivity [W/m·K]	10.006–32.992	Shackelford and Alexander (2001)
Pilling-Bedworth ratio	2.07	Latu-Romain et al. (2019)
Melting temperature [K]	2603	Shackelford and Alexander (2001)

The P-B ratio is the ratio of the volume of the elementary cell of a metal oxide to the volume of the elementary cell of the corresponding metal.

2.9. Failure criteria

Burst data is essential for fuel performance codes to predict cladding failure. Burst stress data on Cr-coated Zircaloy cladding have been compiled from various references. Unfortunately, no information regarding fracture and rupture strain has been found. Fig. 9 displays the engineering burst hoop stress as a function of the burst temperature from all the available datasets in the open literature.

Table 3 summarizes the characteristics of the coated samples used in each test. At this point, no direct comparison can be made with the stress limit used in TRANSURANUS as all the experimental data is provided in terms of engineering stress, while the correlation in the code relies on a true measure of stress. However, Section 3.2 outlines how some of the above burst data can be converted into true stress, enabling the derivation of a stress limit for Cr-coated Zircaloy. This was not included in the present section to maintain independence between the available data and the conversions required for a particular code implementation.

3. Code extension to Cr-coated Zircaloy simulation

3.1. Selection of modelling approach

When extending fuel performance codes to simulate coated claddings, there are two basic approaches to consider (Geelhood and Luscher, 2019). The first approach involves modelling the coating and the cladding independently. This requires the characterization of thermo-mechanical properties specific to the pure coating material and modelling the phenomena occurring at the interface between the substrate and the coating. Notably, based on available open literature, all fuel performance simulations involving Cr-coated Zircaloy have adopted this approach (Dunbar et al., 2024; Ma et al., 2021; Ševeček et al., 2018;

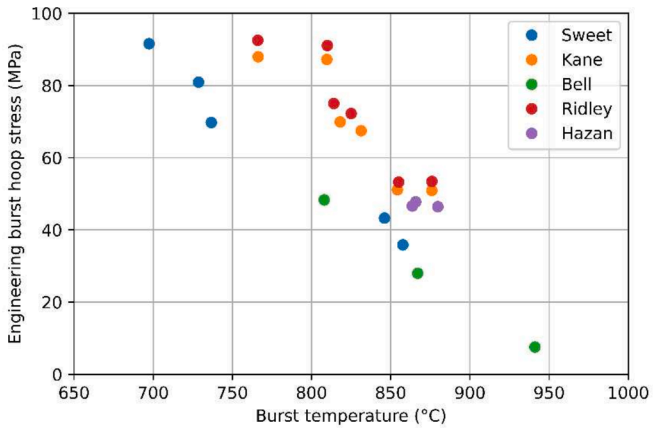

Fig. 9. Engineering burst hoop stress as a function of burst temperature.

Table 3
Basic characterization of coated cladding samples utilized in each burst test.

Material	Deposition method	Coating thickness (μm)	Reference
Cr-coated Zry-4	HiPIMS	7	Sweet et al. (2022)
Cr-coated Zry-4	HiPIMS	6.2	Kane et al. (2023)
Cr-coated Zry-4	HiPIMS	6.8	Ridley et al. (2023a)
Cr-coated Zry-4	Cold spray	25	Hazan et al. (2021)
Cr-coated ZIRLO	HiPIMS	4.4	Bell et al. (2022)

HiPIMS: High power impulse magnetron sputtering.

Sweet et al., 2022; Wagih et al., 2018). However, none of these simulations include specific models for the cladding-coating interface.

Alternatively, the second approach views the coated cladding as a composite material and aims to establish effective correlations. For instance, the creep properties of both the coating and the cladding are combined into an effective creep rate. These effective correlations can be derived by testing representative coated specimens and either (i) fitting the data to a specific function or (ii) adjusting the standard Zr-based cladding correlations using a corrective factor. Adopting this second approach offers a more straightforward path, potentially eliminating the need for additional modelling efforts. Furthermore, treating the coated cladding as a single material might provide a basis for ignoring the coating in the analyses and relying on existing cladding properties, except for corrosion (Geelhood and Luscher, 2019).

As highlighted in Section 2, the open literature contains only two effective correlations for Cr-coated cladding, which characterize the thermal creep strain rate of Cr-coated Zircaloy-4 (Ridley et al., 2023b). However, other effective creep correlations have been proposed by industrial companies (Vidal et al., 2022) or within the framework of international projects. In the IAEA/CRP ATF-TS, a correlation has been derived from burst tests on Cr-coated Optimized ZIRLO, while in the H2020 Euratom project R2CA, a factor of 0.5 has been added to the Zircaloy creep strain rate in DRACCAR to simulate coated claddings (Pouillier, 2023).

In light of these two approaches, this section aims to justify why, based on the available data, the authors recommend the independent modelling of the coating and the cladding.

Experimental studies indicate that Cr coatings enhance the thermal creep resistance of fuel rods (Brachet et al., 2016; Hazan et al., 2021; Ridley et al., 2023a; Ševeček et al., 2021; Walters et al., 2021). Nevertheless, effective creep correlations may not necessarily capture this improvement when compared to the standard Zircaloy creep correlation in a specific code. Fig. 7 illustrates this discrepancy for TRANSURANUS below 860 °C, which is not entirely unexpected. That is, introducing a 10 to 20 μm thick Cr coating has indeed been shown to strengthen the cladding at high temperatures, potentially reducing the creep rate by a factor between 1.5 and 2 (Chalupová et al., 2019). In the field of fuel performance modelling, however, this variation likely falls within the uncertainty range of the Zircaloy creep correlation (Feria et al., 2024), and thus meaningful comparisons become challenging. In other words, merely adjusting the coverage factor when selecting creep data during model derivation might introduce larger variations than those attributed to the Cr coating. In that case, the intrinsic strengthening effect of the coating could not be differentiated from the bias of the Zircaloy creep correlation.

Moreover, the data utilized to derive Zircaloy creep correlations may have been obtained from samples that are no longer representative of the current state-of-the-art cladding standards, given the ongoing refinements in fabrication techniques and alloy composition. Specifically, the thermal creep correlation included in TRANSURANUS and FRAPTRAN-TUmech originates from the REBEKA separate effects tests conducted in the 1980 s (Markiewicz and Erbacher, 1988). Consequently, comparing creep correlations derived from REBEKA samples with those from contemporary uncoated samples, even if experimental data were obtained under identical conditions, could lead to discrepancies potentially exceeding a factor of 2. All of the above is to say that, in the field of cladding creep modelling, it should not be surprising to leave out an improvement of merely a factor between 1.5 and 2.

The above arguments emphasize the recommendation to model the coating and the cladding, independently rather than treating them as a composite material. The recommended approach helps avoid unrealistic simulation outcomes that deviate from experimental observations, especially in terms of high-temperature strength. While it is true that modelling the composite material using a reduction factor (i.e., <1) applied to the Zircaloy creep correlation (e.g., 0.5 in the DRACCAR code) can prevent unrealistic results, employing a separate creep law for the coating provides a more realistic representation, as it allows for the consideration of temperature and stress dependencies specific to the coating creep rate. Furthermore, it aligns with the current trend towards more mechanistic modelling, enabling better consideration of factors such as the coating material composition and thickness.

3.2. *Implementation of the selected modelling approach*

The TRANSURANUS fuel performance code (European Commission, 2023) and the FRAPTRAN-TUmech suite (Aragón et al., 2024) have been extended to simulate Cr-coated Zircaloy by independently modelling the coating and the cladding. An important clarification concerns the choice of the starting framework for the FRAPTRAN extension. Instead of building upon the most recent version provided by its developers, FRAPTRAN-2.0 (Geelhood et al., 2016), the foundation lies on the FRAPTRAN-TUmech suite developed in collaboration between CIEMAT and JRC-Karlsruhe for conventional Zircaloy cladding. TUmech is a simplified standalone version of the mechanical model in TRANSURANUS coupled with FRAPTRAN-2.0 to enhance its predictive capabilities for the cladding response under LOCA conditions. The extension of two analytical tools to simulate coated cladding further supports the insights gained in this study, reducing their sensitivity to specific modelling aspects within each code.

The cladding mechanical model in FRAPTRAN-2.0 is based on a single node radial nodalization. While a single node enables the definition of effective correlations for the coated cladding, it lacks the capability for separate modelling of the coating and the cladding. The use of TUmech, with its multi-nodal radial representation of the cladding, as opposed to the default mono-nodal FRACAS-I (Bohn, 1977) and BALON2 (Hagrman, 1981) models in FRAPTRAN-2.0, facilitates the implementation of the selected modelling approach.

The material models and correlations implemented for the coating correspond to those detailed in Section 2, except for emissivity. This property has been omitted from the implementation because it solely affects the gap thermal calculation in TRANSURANUS and FRAPTRAN-TUmech, and the coating is applied to the outer surface of the cladding.

An essential aspect to highlight regarding the FRAPTRAN-TUmech extension is the limitation on implementing certain coating properties. These can only be added if considered within TUmech (i.e., are relevant to the mechanical analysis). Other material properties are calculated for the entire coated cladding from the baseline Zircaloy correlations in FRAPTRAN-2.0, sourced from the MATPRO database (Luscher et al., 2015). The material properties considered in TUmech include the thermal expansion coefficient, elastic constants, thermal creep, and failure criteria. Additionally, the high-temperature oxidation model derived for Cr has been implemented. As a result, in the FRAPTRAN-TUmech simulations, the thermal conductivity and specific heat correlations for Zircaloy are maintained for the coated cladding. The validity of this simplification is justified by the higher thermal conductivity of pure Cr, which will not impact heat transfer, and the small volumetric/

mass fraction of the coating, thus resulting in a negligible impact on its specific heat capacity.

Finally, it is worth noting that neither FRAPTRAN-2.0 nor FRAPTRAN-TUmech account for irradiation swelling and creep; however, their impact under LOCA conditions is negligible.

Next, the assumptions and limitations specific to the extension of TRANSURANUS and FRAPTRAN-TUmech to simulate Cr-coated Zircaloy cladding are listed:

1. Conservatively, the melting temperature of the Cr coating is assumed to be the temperature of the Zr-Cr eutectic reaction, i.e., around 1332 °C (1605.15 K) (Brachet et al., 2020).
2. Permanent (mechanical) deformation is solely attributed to thermal creep strains. The yield strength of the coating is set to an arbitrarily large value to prevent entering the plastic deformation regime. Even if a model for the instantaneous plasticity of the Cr coating were implemented, no plastic strains would be calculated in the Zircaloy substrate. This is because both TRANSURANUS and FRAPTRAN-TUmech currently lack an instantaneous plasticity model for Zircaloy. Future code developments are envisaged to address this limitation.
3. No dedicated hydrothermal corrosion or hydrogen pickup models have been implemented. The kinetics for both processes have been set to zero based on the minimal corrosion observed experimentally under normal operating conditions (USNRC, 2020).
4. When selecting a stress-based cladding failure criterion, overstress is assumed if the average true hoop stress in the cladding (or coated cladding) exceeds the defined stress limit. Therefore, the rigorous implementation of a stress limit in both codes requires a true stress definition. The conversion from engineering burst hoop stress to true burst hoop stress is feasible solely for the datasets provided by Ridley et al. and Hazan et al., as they also reported post-burst strain data. Both Ridley et al. and Hazan et al. determined the maximum circumferential (engineering) strain at burst, which is defined as:

$$\varepsilon_{\theta,eng} = \frac{l_B - l_0}{l_0} \tag{9}$$

where l_B represents the maximum perimeter at burst and l_0 denotes the initial (axially uniform) perimeter. The conversion from engineering strain to true strain is expressed as:

$$\varepsilon_{\theta,tru} = \ln\left(1 + \varepsilon_{\theta,eng}\right) \tag{10}$$

The above expression enables the calculation of the true hoop stress in a thin-walled cylinder:

$$\sigma_{\theta,tru} = \sigma_{\theta,eng}\left(1 + \varepsilon_{\theta,tru}\right)^2 = \frac{\Delta p \cdot r_{in,0}}{t_0}\left[1 + \ln\left(1 + \varepsilon_{\theta,eng}\right)\right]^2 \tag{11}$$

Here, Δp is the rod overpressure at burst, while $r_{in,0}$ and t_0 are the initial inner radius and thickness of the cladding. An exponential fit has been applied to the obtained dataset (true burst hoop stress vs. burst temperature), resulting in Eq. (12), which is also plotted in Fig. 10. The burst stress at the lowest temperature in the Ridley et al. and Hazan et al. experimental datasets (766 °C) is applied at all temperatures below it.

$$\sigma_{\theta B}[\mathrm{MPa}] = 8.5716 \cdot 10^7 \cdot \exp\left(-1.2133 \cdot 10^{-2} T\right) \tag{12}$$

where the temperature is expressed in K.

Fig. 10 includes the stress-based burst criterion from TRANSURANUS for generic Zircaloy (Neitzel and Rosinger, 1980). Given the absence of true burst hoop stress versus burst temperature data in the original reference, the data used in deriving the stress limit of FRAPTRAN-2.0 (Geelhood et al., 2016) is also plotted to underline the large spread of the data for conventional Zircaloy.

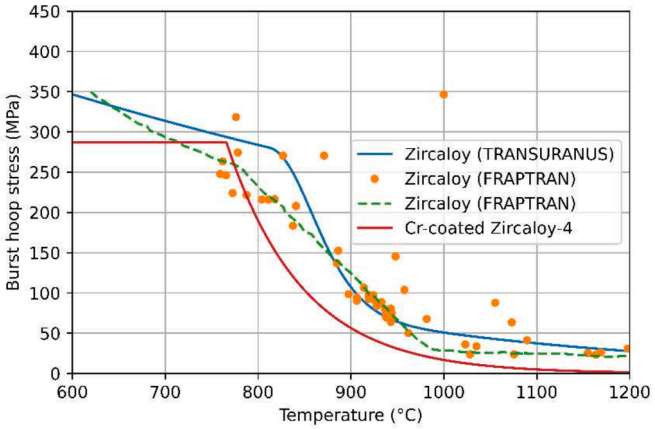

Fig. 10. True burst hoop stress as a function of temperature.

5. As an alternative to the previous stress limit, a failure criterion based on the maximum allowable strain rate has been implemented. Plastic instability is assumed to occur when the effective creep strain rate exceeds 100 h^{-1} (2.78 %/s). This threshold has already been used as a failure criterion in other fuel performance analyses involving Cr-coated Zircaloy cladding (Sweet et al., 2022) and is considered to yield accurate burst time predictions. However, the cladding strain profile might be significantly underestimated (Capps and Sweet, 2022).
6. Phenomena specific to the cladding-coating interface (e.g., Zr-Cr interdiffusion) are not modelled.
7. Regarding the radial nodalization of the coating, the default configuration allocates a single coarse node at the periphery of the cladding. The user may choose the number of fine zones within that coarse zone. For all the simulations shown below, three fine zones are considered.

An essential discussion arises from the comparison in Fig. 10. All burst data on Cr-coated Zircaloy available in the literature (Bell et al., 2022; Hazan et al., 2021; Kane et al., 2023; Ridley et al., 2023a; Sweet et al., 2022) consistently demonstrate higher burst temperatures than those measured for Zircaloy in the same studies. Despite the experimentally observed high-temperature strengthening effect of the coating, a higher stress limit is not evident in Fig. 10. This apparent discrepancy between experimental data and correlation derivation is exacerbated by the fact that, even considering the substantial spread in the FRAPTRAN-2.0 burst data, the stress limit correlation derived for Cr-coated Zircaloy consistently remains lower at any temperature above 800 °C.

A potential explanation lies in the definition of true stress in Eq. (11). All the aforementioned experimental studies report the engineering hoop stress at burst ($\sigma_{\theta,eng}$). However, when converted to true burst hoop stress ($\sigma_{\theta,tru}$), the previous quantity must be multiplied by a factor that increases with the true hoop strain at burst, related to the balloon size. Burst test results indicate a reduced balloon circumference coupled with a smaller burst opening of Cr-coated cladding compared to uncoated Zr-based cladding (Walters et al., 2021), resulting in a lower value of $\varepsilon_{\theta,tru}$ in Eq. (11). The comparison in Fig. 10 suggests that the reduction in balloon size (i.e., lower true hoop strain at burst) dominates over the increased engineering hoop stress at burst, hence yielding a lower stress limit when using a true stress definition in fuel performance codes. Nevertheless, definite conclusions cannot be drawn due to the limited availability of burst data on coated cladding suitable for deriving true stress limits.

Finally, to enable a comparison between simulations based on the independent modelling of the coating and cladding versus the composite material approach, an effective creep rate correlation has been implemented into TRANSURANUS. The chosen correlation adopts a Norton

law derived by Ridley et al. (2023b) with the strength coefficient calculated from isobaric tests conducted at a 5 °C/s heating rate (see Table 1), which better represents the heat-up phase of a LOCA scenario compared to isothermal tests.

$$\dot{\varepsilon}_\theta = 124\sigma^{6.12}\exp\left(-\frac{287\,\mathrm{kJ/mol}}{RT}\right) \tag{13}$$

However, as mentioned in Section 2.7, the strength coefficient presented by Ridley et al. applies solely to circumferential and not to effective strain, the quantity computed within the code. Thus, a conversion becomes necessary. In the frame of the thin wall approximation, and under the assumption of axisymmetric and isotropic mechanical performance, the relation between effective ($\dot{\varepsilon}$) and hoop ($\dot{\varepsilon}_\theta$) strain rates in a hollow cylinder can be expressed as:

$$\dot{\varepsilon} = z\frac{2}{\sqrt{3}}\dot{\varepsilon}_\theta \tag{14}$$

z represents a geometry-dependent correction factor defined as:

$$z = \frac{1+\frac{t_0}{2r_0}}{\left(1+\frac{t}{r_0}\right)^2} \tag{15}$$

where t is the actual thickness of the cladding (i.e., in its deformed geometry), and r_0 and t_0 denote the position of a specific radial node in the undeformed cladding geometry and the thickness of the undeformed cladding, respectively.

4. Results and discussion

The extensions of TRANSURANUS and FRAPTRAN-TUmech have been used to predict the behaviour of coated claddings under conditions that mimic two LOCA tests: QUENCH-L1 rod 4 (an out-of-pile bundle test on unirradiated Zircaloy cladding) and IFA-650.10 (an in-pile single rod test on high-burnup Zircaloy-UO_2 fuel rod). These scenarios offer an increasing degree of complexity that enables a gradual verification of the code extensions. The predictions for uncoated cladding using the original versions of the codes have also been included in the discussion, providing a comparative performance analysis.

Table 4 summarizes the test rod fabrication data and the burnup (when applicable) for the selected scenarios. Further details on the experimental setup and sequence of each test are given in the dedicated subsections. In all simulations involving Cr-coated Zircaloy, a 20 μm thick Cr coating is added on the surface of the cladding.

Table 4
Test rod specifications.

Test	QUENCH-L1 rod 4	IFA-650.10
Pellet		
Material	ZrO_2	UO_2
Diameter [mm]	9.15	8.19
Length [mm]	11	13.78
Density [% TD]	–	95.32
Cladding		
Material	Zircaloy-4	Zircaloy-4
Outer diameter [mm]	10.75	9.5
Wall thickness [μm]	725	570
Fuel rod		
Burnup [MWd/kgU]	0	61
Active length [mm]	–	440
Pellet-cladding gap [μm]	75	84
Plenum volume [cm^3]	0	17
Fill gas	100 % Kr	95 % Ar + 5 % He
Fill pressure [MPa]	5.5 (@ 527 °C)	4 (@ 25 °C)
Pitch [mm]	14.3	–

4.1. QUENCH-L1 rod 4

In the QUENCH-L1 experiment, a mixture of superheated steam and argon was introduced at the base of a test bundle comprising 21 electrically heated rods, each approximately 2.5 m long. The heaters were encased in annular ZrO_2 pellets. The system pressure within the test section remained at about 0.3 MPa. Before the transient phase, each fuel rod was individually pressurized with krypton to 5.5 MPa. To control the internal pressure in real-time, a dedicated gas supply system was connected to the lower end of each rod, comprising a pressure valve, a pressure transducer, and an adjustable compensation volume. The latter preserved the initial free volume throughout the transient, compensating for the lack of empty plenums within the rods. Additionally, thermocouples were attached at 17 different elevations and orientations on the outer surface of the cladding for temperature monitoring. The transient sequence involved a heat-up phase, elevating temperatures from 570 to 1100 °C at a peak heating rate of 7 °C/s over 90 s, followed by a 120 s cooling phase. The test was concluded by water quenching (Stuckert et al., 2018).

In view of the online pressure control, the rod internal gas pressure during the simulation has been imposed in accordance with experimental data, albeit in a simplified form (IAEA, 2019). As noted in (Stuckert et al., 2012), cladding deformation consistently began at approximately 250 mm and concluded at 1250 mm elevation across all rods. Thus, the results from TRANSURANUS and FRAPTRAN-TUmech are specifically obtained for this segment of rod 4. More precisely, the fuel rod is nodalized into 13 equally-sized axial nodes, spanning from 100 mm to a maximum elevation of 1400 mm. The evolution of the cladding outer temperature at each axial node has been prescribed using thermocouple data (IAEA, 2019). Fig. 11 illustrates the evolution of the rod internal gas pressure and the range of cladding surface temperatures over the entire length of the segment. A single coarse zone comprising five fine zones has been defined for the radial nodalization of the cladding.

The evolution of the cladding permanent hoop strain at the burst node is plotted in Fig. 12. Cladding failure is indicated by the termination of the mechanical calculation when the effective creep rate exceeds 100 h^{-1} (2.78 %/s), which marks the onset of plastic instability. Throughout the entire transient, the two codes exhibit perfectly consistent predictions. Indeed, this consistency serves as confirmation of the correct coupling of TUmech with FRAPTRAN-2.0. In the QUENCH-L1 rod 4 scenario, the cladding mechanical problem simplifies to that of a closed cylindrical tube subjected to external and internal pressure, which both codes address using the same formulation, numerical algorithm, and material property correlations. Additionally, they share identical boundary conditions (i.e., cladding outer temperatures and coolant pressure). Consequently, achieving identical results is expected.

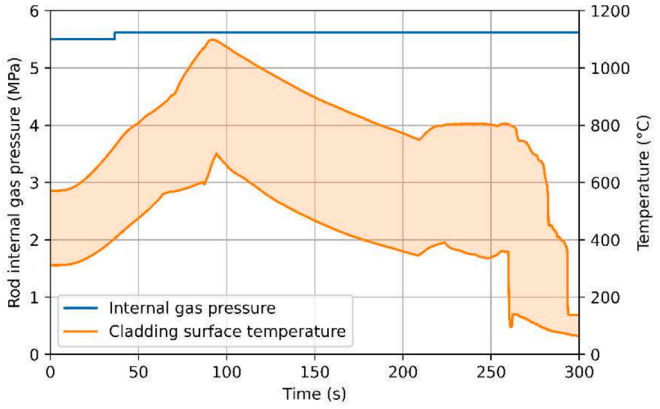

Fig. 11. Time-dependent boundary conditions for the QUENCH-L1 rod 4 simulation.

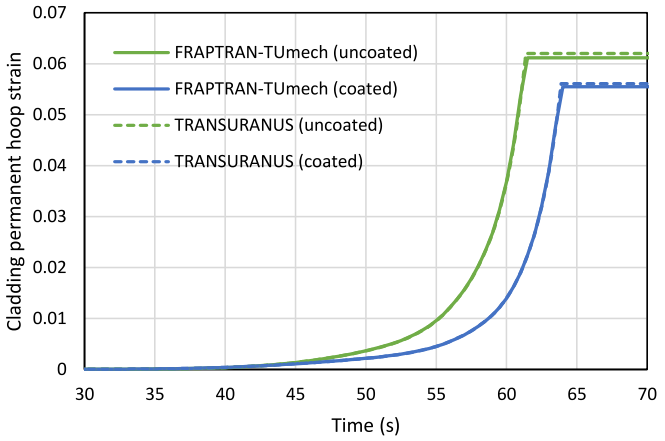

Fig. 12. Cladding permanent hoop strain as a function of time.

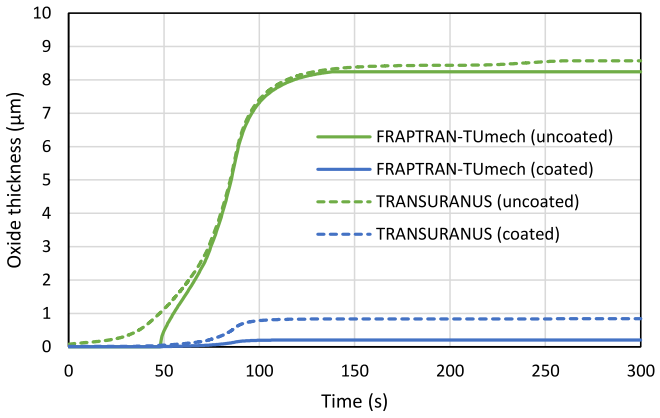

Fig. 13. Oxide layer thickness as a function of time.

The 1 % difference at failure is likely due to variations in the time step size used by each code, resulting in failure occurring at slightly different times.

Next, the impact of the Cr coating on the performance of the Zircaloy-4 cladding is examined. As temperature rises, the increasing ductility of the internally pressurized cladding leads to progressive ballooning. During the process of permanent deformation, the volume of the cladding is conserved, resulting in wall thinning and a subsequent rapid increase in hoop stress. Both TRANSURANUS and FRAPTRAN-TUmech simulations indicate that the addition of a 20 μm thick Cr coating postpones the burst time by 4 % (2 s). Most of this delay can be attributed to the reduced thermal creep rate associated with the Cr coating, which appreciably influences the stress and strain dynamics in the cladding. However, the increased thickness of the coated cladding also contributes noticeably (25 % of the total delay). This observation is based on the outcome of an additional simulation not shown in Fig. 12, where the coating material was replaced with Zircaloy instead of Cr (equivalent to a 20 μm thicker Zircaloy cladding). Regarding post-burst strains, there are no significant differences between uncoated and coated cladding (less than 1 %). It is important to note, though, that the latter result stems from adopting a plastic instability failure criterion.

The rationale for employing a failure criterion based on plastic instability instead of overstress is as follows. While both codes utilize the same formulation and iterative numerical method for the cladding mechanical calculation, TRANSURANUS includes a time-step control mechanism. This feature automatically reduces the time step size when encountering specific criteria that could compromise the convergence of the method. Since the development of TUmech is relatively recent, the adaptative time step control has not yet been integrated. Therefore, without limiting the maximum allowable strain rate, convergence issues arise before reaching the proposed stress limit. The impact of employing a plastic instability versus an overstress failure criterion on the burst time and the post-burst strain is evaluated in Section 4.3.1.

An additional simulation of coated cladding has been conducted. In this simulation, the thermal creep of the coating was calculated using the generic Zircaloy correlation in TRANSURANUS, while other coating properties were described using correlations for pure Cr, as in the previous coated cladding simulation. The results confirm that the difference between coated and uncoated claddings in terms of burst time arises solely from their distinct thermal creep rates. Therefore, other material properties may be reasonably approximated using Zircaloy properties without loss of accuracy.

Fig. 13 shows the evolution of the outer oxide layer thickness at the burst node. Both coated and uncoated claddings follow trends consistent with the initial heating phase, starting at the onset of the transient and continuing until 90 s. However, in the FRAPTRAN-TUmech simulations, the high-temperature steam oxidation model is activated only when the average cladding temperature, or the outer cladding temperature if a coating layer is present, reaches 800 °C, in line with the original FRAPTRAN-2.0 code. Beyond 90 s into the transient, as the temperature begins to decline, the growth rate of the oxide layer decreases accordingly. For FRAPTRAN-TUmech, the oxidation calculation ceases once the temperature falls below 800 °C. It is important to highlight that the high-temperature oxidation models for both coated and uncoated claddings are applied across all transient phases, regardless of the coolant quality.

Regarding the effect of the Cr coating, by the end of the test, the oxide layer on the uncoated cladding is roughly 10 times thicker according to TRANSURANUS and 40 times thicker according to FRAPTRAN-TUmech when compared to the coated cladding. This result aligns with the notably enhanced resistance of Cr to high-temperature steam oxidation. In both simulations, the thickness of the oxide layer on the coated cladding remains below 1 μm, indicating that only a small fraction of the coating (< 10 %) is consumed by oxidation.

4.2. IFA-650.10

The Halden IFA-650.10 experiment is an in-pile single rod test on fuel behaviour under simulated LOCA conditions (Lavoil, 2010). It employed a 440 mm segment cut from a standard PWR fuel rod previously irradiated in a commercial reactor to an average burnup of 61 MWd/kgU. The test was performed at low constant fission power (1.37 kW/m, simulating the decay power immediately following a reactor scram) to achieve the desired conditions for cladding ballooning and high-temperature oxidation. The initiation of the blow-down phase involved opening the valves that allowed the water to flow from the bottom of the test rig to the dump tank. As a result, the test rig pressure rapidly decreased from 7 MPa to around 4.5 MPa, depleting most of its water content within 70 s. The presence of stagnant superheated steam around the test rod led to insufficient cooling, triggering the heat-up phase. The peak cladding temperature reached 850 °C and the average temperature increase rate during the heat-up was around 8 °C/s. The test was concluded by reactor scram 417 s following the onset of the blowdown.

Unlike the QUENCH-L1 scenario, the simulation of the IFA-650.10 test necessitates a base irradiation simulation to characterize the state of the fuel rod at the onset of the transient. For this purpose, preceding each LOCA simulation with FRAPTRAN-TUmech, a base irradiation simulation was conducted using the default version of the steady-state fuel performance code FRAPCON-4.0 (Geelhood et al., 2014). This also holds for the coated cladding base irradiation simulation, given that the TUmech mechanical module has not yet been coupled with FRAPCON-4.0.

It is important to recall that the multi-nodal formulation of TUmech is indispensable for independently modelling the cladding and the

coating. However, the current version cannot handle closed-gap regimes, which occur under normal operating conditions from relatively modest burnups. Consequently, coupling the current version of TUmech with FRAPCON-4.0 (developed to perform steady-state calculations of fuel rods under normal operating conditions) would not provide valid predictions.

Nonetheless, simulating the base irradiation of coated cladding as if it were uncoated cladding offers a reasonable approximation for most material properties. This is justified by the fact that, under normal operating conditions, the most significant differences between coated and uncoated claddings are the enhanced fretting performance, improved wear resistance, and negligible corrosion exhibited by the coating (USNRC, 2020). Wear and fretting phenomena are not addressed in FRAPCON-4.0 or TUmech, making modifications in this aspect unfeasible, and the corrosion of coated cladding has been set to zero during base irradiation.

On the other hand, TRANSURANUS has the capability to simulate fuel behaviour under both normal operation and accident conditions, enabling the execution of a single code run that encompasses both the base irradiation and subsequent LOCA test.

Fig. 14 displays the measured test rig pressure and the range of cladding surface temperatures along the active length of the rodlet (IAEA, 2019). As in the QUENCH-L1 scenario, the T/H boundary conditions provided to each code are identical. In both codes, the cladding is nodalized into 20 axial nodes and nine radial fine zones enclosed within a single coarse zone. The pitch distance has been set to an arbitrarily large value, considering the absence of adjacent rods in the experimental setup.

The figures of merit considered in this scenario are the rod internal gas pressure and the cladding permanent hoop strain at the burst node.

Fig. 15 shows the rod internal gas pressure evolution. A detailed discussion on the origin of the differences between TRANSURANUS and FRAPTRAN-TUmech for uncoated cladding is beyond the scope of this paper and has been previously addressed in Aragón et al. (2024). In short, the main source of discrepancy lies in the calculation of the plenum volume. While the initial cold-state plenum volume is consistent across simulations, its evolution is calculated using different models. Additionally, the correlation used to estimate the axial elongation of the fuel stack, and especially the cladding, due to thermal expansion significantly contributes to the differences observed between TRANSURANUS and FRAPTRAN-TUmech.

The focus here is on assessing the impact of adding a 20 μm thick Cr coating. As expected, the lower creep strain rate of the coating slows down cladding deformation. This delay becomes evident in the time taken to reach the maximum rod internal pressure, particularly in the FRAPTRAN-TUmech simulation, as it marks the point where the free volume gain from cladding deformation starts dominating over internal gas heating. Fig. 6 clearly shows that, under the same conditions, Cr

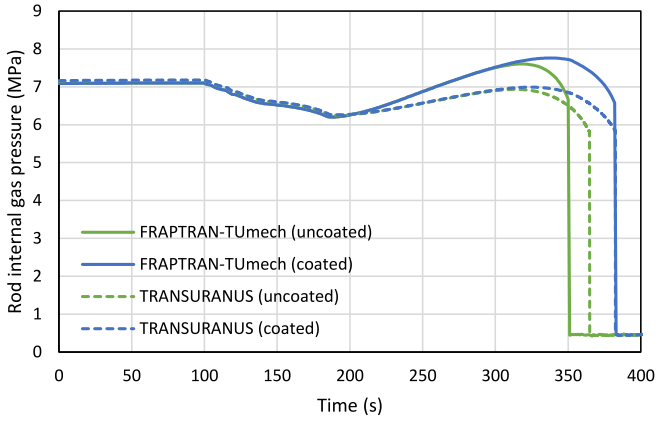

Fig. 15. Rod internal gas pressure as a function of time.

undergoes creep deformation at a much lower rate than Zircaloy. As a result, while the rod internal gas pressure eventually increases in all simulations due to rising temperatures, the faster increase in free volume (caused by creep deformation) in the Zircaloy simulations leads to an earlier offset of this pressure increase. On the other hand, Cr-coated Zircaloy deforms more slowly, and the maximum rod internal gas pressure is reached later in the transient.

The slower transition to the free volume dominance breakpoint, combined with a lower deformation rate thereafter, results in a delayed burst time compared to uncoated cladding. Burst is indicated by the rapid internal pressure drop to match the test rig pressure. TRANSURANUS and FRAPTRAN-TUmech predict delays of 5 % (18 s) and 9 % (32 s) for coated cladding, respectively.

Finally, the evolution of the cladding permanent hoop strain at the burst node is plotted in Fig. 16. The time scale on the x-axis has been adjusted for better visualization of the results. As in the QUENCH-L1 simulation, and due to the utilization of the same plastic instability failure criterion for both coated and uncoated cladding, no conclusions can be drawn regarding post-burst strains. Additionally, it is worth noting that the use of such a failure criterion tends to underestimate strains (Capps and Sweet, 2022).

4.3. Sensitivity analyses with TRANSURANUS

After introducing the scenarios simulated with the extended fuel performance tools, this section presents two sensitivity analyses. One is conducted to quantify the deviations introduced by the choice of cladding failure criteria, and the other to justify specific aspects of the modelling approach. The implementation of coatings into TRANSURANUS and FRAPTRAN-TUmech was not a straightforward process;

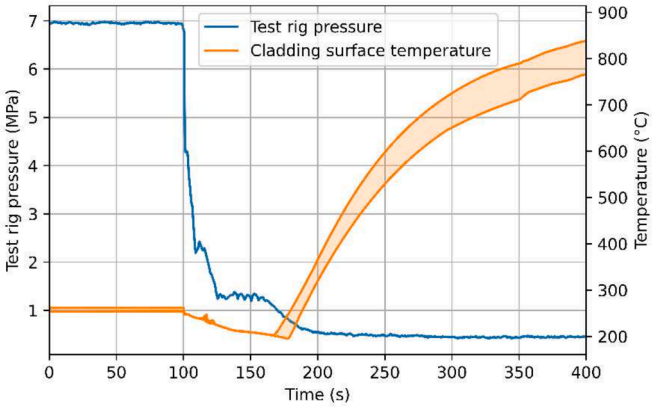

Fig. 14. Time-dependent boundary conditions for the IFA-650.10 simulation.

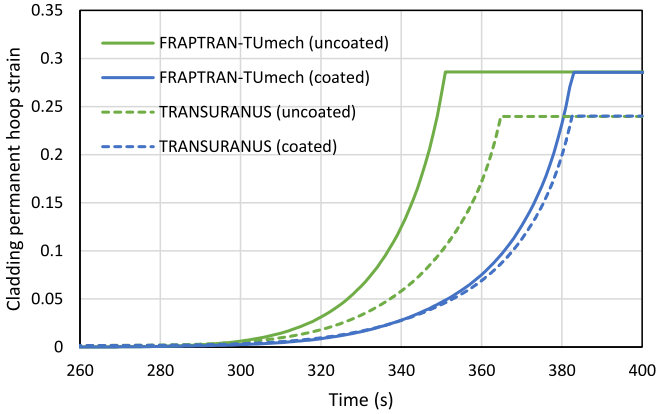

Fig. 16. Cladding permanent hoop strain as a function of time.

rather, it was informed by the insights gained from these sensitivity analyses. Both analyses have been carried out with TRANSURANUS under the conditions of the IFA-650.10 test.

4.3.1. Impact of failure criteria

This analysis evaluates the impact of the failure criterion on burst time and post-burst strains. Assessing post-burst strains is essential to determine whether the coated cladding simulations can reproduce the smaller balloon size observed experimentally. However, the adoption of a plastic instability failure criterion in the previous simulations hinders reaching valid conclusions. Conversely, the use of a true stress limit enables quantification of the differences between coated and uncoated cladding in this regard.

Two additional simulations were performed, assuming overstress if the average true tangential stress exceeds the stress limits displayed in Fig. 10. In the subsequent figures, results are presented for the simulations using the plastic instability (dashed line corresponding to the results shown in Section 4.2) and the overstress criterion (dotted line). It is important to note that the same comparison with FRAPTRAN-TUmech is not feasible due to the absence of a time-step control, which requires limiting the maximum allowable strain rate (i.e., using a plastic instability criterion), as previously discussed.

As illustrated in Fig. 17, the two curves for each cladding design coincide until reaching the plastic instability threshold, which consistently precedes the stress limit. As mentioned in Section 4.2, the addition of a 20 μm thick coating results in a 5 % (18 s) delay in burst time when applying the plastic instability failure criterion. Conversely, when using the overstress criteria outlined in Fig. 10 for coated and uncoated cladding, their burst times increase by approximately 5.5 s. Therefore, the magnitude of the delay attributed to the coating remains consistent. It is worth highlighting that observing such minimal variations in burst time across different failure criteria aligns with findings from other modelling studies (Feria et al., 2024).

In contrast, Fig. 18 reveals that, when applying a stress limit, the coated cladding exhibits significantly lower strains (36 % reduction) compared to the uncoated cladding.

4.3.2. Assessment of effective modelling approach

The current sensitivity analysis aims to assess the differences resulting from the selection of modelling approach for simulating coated claddings. As demonstrated earlier, the impact of coating properties other than creep can be disregarded without compromising accuracy. Thus, the effective modelling approach has been exclusively applied in the description of thermal creep, while Zircaloy correlations have been used for all other material properties except for high-temperature oxidation.

Fig. 19 shows the evolution of the rod internal gas pressure. Cladding failure is assumed at the plastic instability threshold for both coated and uncoated claddings. The orange curve (coated*) represents a coated cladding simulation where the coating and the cladding are treated as a composite material. It differs from the uncoated cladding simulation in the thermal creep correlation (Eqs. (13)-(15) are used instead of the generic Zircaloy correlation), the cladding thickness (i.e., an additional 20 μm are added to account for the coating), and the high-temperature oxidation model. Note that the blue and green curves were previously included in Fig. 15.

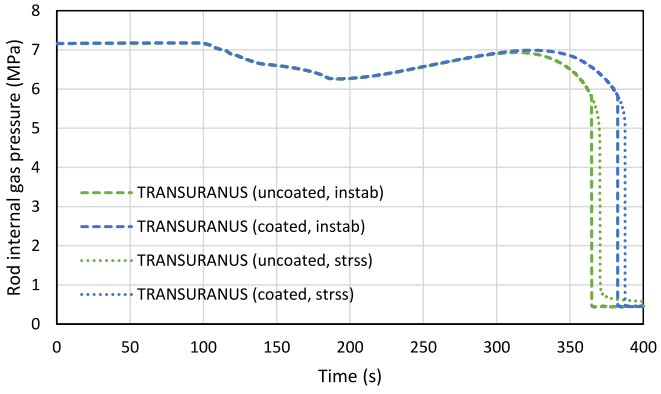

Fig. 17. Rod internal gas pressure evolution for IFA-650.10 with TRANSURANUS.

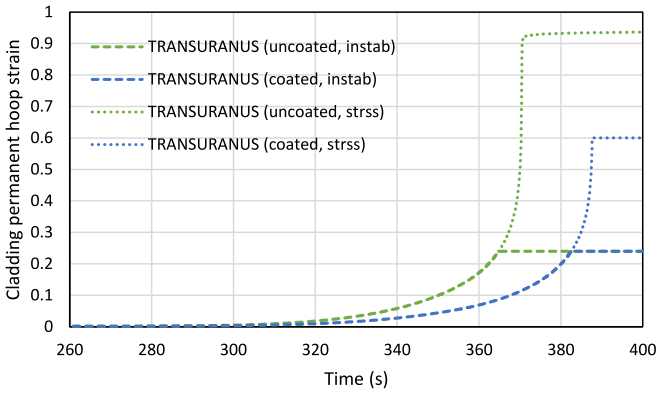

Fig. 18. Cladding permanent hoop strain evolution for IFA-650.10 with TRANSURANUS.

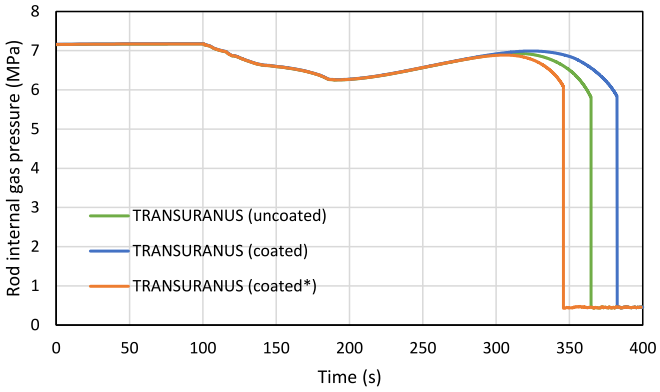

Fig. 19. Rod internal gas pressure evolution for IFA-650.10. TRANSURANUS (coated*) corresponds to a simulation of coated cladding using an effective thermal creep correlation.

The IFA-650.10 case is a clear example of the potential drawback of implementing effective coated cladding properties into fuel performance codes. The predicted burst time for coated cladding, simulated with an effective creep correlation, occurs roughly 20 s earlier than for uncoated cladding, despite the greater thickness of the former. This discrepancy with experimental observation underscores the importance of approaching the adoption of effective creep correlations with careful consideration. Of course, these results are contingent on the specific code and scenario considered.

A more meaningful comparison of code predictions could be achieved if the same experimentalists who derived effective creep correlations for coated samples also conducted analogous experiments on uncoated samples, using the same experimental setup, testing procedure, and Zircaloy material.

5. Conclusions

This paper introduces the extension of the TRANSURANUS fuel performance code and the FRAPTRAN-TUmech suite to simulate Cr-coated Zircaloy. For that purpose, a review of models and correlations for pure Cr, as well as effective coated cladding properties, relevant to

fuel performance modelling has been conducted. Additionally, a discussion on the two basic modelling approaches to coating simulation is presented to justify the selected code implementation strategy. The extended tools are then applied to simulate the behaviour of coated and uncoated cladding under two scenarios, which mimic the conditions of QUENCH-L1 rod 4 (fresh cladding) and IFA-650.10 (high burnup fuel rod) LOCA tests.

The following conclusions can be drawn from the outcome of the simulations:

- The independent modelling of the coating and cladding is recommended over treating the coated cladding as a composite material, as the latter approach may result in unrealistic predictions that deviate from experimental observations. This mechanistic approach aligns with current trends in high-fidelity modelling and should better account for variations in coating material compositions, thickness, and fabrication techniques.
- The thermal creep of the coating plays a fundamental role in the overall behaviour of coated cladding during LOCA conditions. The impact of other thermo-mechanical properties may be neglected without loss of accuracy.
- The addition of a 20 μm Cr coating does not result in any significant delay in burst time relative to uncoated cladding (less than 10 %). Conversely, the predictions of post-burst strains based on true overstress criteria align with experimental observations.
- The superior high-temperature steam oxidation resistance of the Cr coating results in a roughly tenfold reduction in oxide thickness.

Additional burst data suitable for deriving true stress limits is recommended to enhance the accuracy of post-burst strain predictions.

Further work includes consideration of Cr diffusion into the substrate at high temperatures, the analysis of scenarios where the complete coating can be oxidised, and a comprehensive validation of TRANSURANUS and FRAPTRAN-TUmech using empirical data from coated fuel rods.

CRediT authorship contribution statement

Pau Aragón: Conceptualization, Software, Investigation, Data curation, Writing – original draft, Visualization. **Francisco Feria:** Investigation, Writing – review & editing, Supervision. **Luis E. Herranz:** Investigation, Writing – review & editing, Supervision. **Arndt Schubert:** Investigation, Writing – review & editing, Supervision. **Paul Van Uffelen:** Investigation, Writing – review & editing, Supervision.

Declaration of competing interest

The authors declare that they have no known competing financial interests or personal relationships that could have appeared to influence the work reported in this paper.

Data availability

Data will be made available on request.

Acknowledgements

This work has been partially supported by the ENEN2plus project (HORIZON-EURATOM-2021-NRT-01-13 101061677) founded by the European Union and the Spanish Nuclear Safety Council (grant for R&D project). It has also received funding from the Euratom research and training programme 2021–2027 through the OperaHPC project under grant agreement n° 101061453, as well as from the APIS project (https://apis-project.eu/) under grant agreement n° 101114673.

References

Adamson, R., Griffiths, M., Patterson, C., 2017. Irradiation Growth of Zirconium Alloys - A Review. ANT International, Tollered, Sweden.

Aragón, P., Feria, F., Herranz, L.E., Schubert, A., 2024. Enhancing cladding mechanical modelling during DBA/LOCA accidents with FRAPTRAN: The TUmech one-dimensional model. PNE under review. Paul Van Uffelen.

Armstrong Harry, P.E., 1964. Dynamic Young's modulus measurements above 1000 C on some pure polycrystalline metals and commercial graphites. Trans. Metall. Soc. AIME 230, 962–966.

Bell, S.B., Graening, T., Evans, A., Kelly, P., Pint, B.A., Kane, K.A., 2022. Burst and oxidation behavior of Cr-coated Zirlo during simulated LOCA testing. J. Nucl. Mater. 564, 153679. https://doi.org/10.1016/j.jnucmat.2022.153679.

Bischoff, J., Vauglin, C., Delafoy, C., Barberis, P., Perche, D., Guerin, B., Vassault, J.P., Brachet, J.C., 2016. Development of Cr-coated Zirconium Alloy Cladding for Enhanced Accident Tolerance, in: Cea-02438699. Presented at the Topfuel 2016 - Light Water Reactor (LWR) Fuel Performance Meeting, Boise, United States.

Bohn, M., 1977. FRACAS: a subcode for the analysis of fuel pellet-cladding mechanical interaction (No. TREE-NUREG-1028, 7219131). EG&G Idaho, Inc. Doi: 10.2172/7219131.

Brachet, J.C., Matthieu Le Saux, V. Lezaud-Chaillioux, M. Dumerval, Q. Houmaire, F. Lomello, F. Schuster, E. Monsifrot, J. Bischoff, E. Pouillier, 2016. Behavior under LOCA conditions of Enhanced Accident Tolerant Chromium Coated Zircaloy-4 Claddings. Presented at the TopFuel 2016 - Light Water Reactor (LWR) Fuel Performance Meeting, Boise, United States.

Brachet, J.-C., Idarraga-Trujillo, I., Flem, M.L., Saux, M.L., Vandenberghe, V., Urvoy, S., Rouesne, E., Guilbert, T., Toffolon-Masclet, C., Tupin, M., Phalippou, C., Lomello, F., Schuster, F., Billard, A., Velisa, G., Ducros, C., Sanchette, F., 2019. Early studies on Cr-Coated Zircaloy-4 as enhanced accident tolerant nuclear fuel claddings for light water reactors. J. Nucl. Mater. 517, 268–285. https://doi.org/10.1016/j.jnucmat.2019.02.018.

Brachet, J.-C., Rouesne, E., Ribis, J., Guilbert, T., Urvoy, S., Nony, G., Toffolon-Masclet, C., Le Saux, M., Chaabane, N., Palancher, H., David, A., Bischoff, J., Augereau, J., Pouillier, E., 2020. High temperature steam oxidation of chromium-coated zirconium-based alloys: Kinetics and process. Corros. Sci. 167, 108537. https://doi.org/10.1016/j.corsci.2020.108537.

Capps, N., Sweet, R., 2022. Characterization of modeling and experimental data inconsistencies from burst testing for high-burnup commercial fuel rod applications. J. Nucl. Mater. 563, 153621. https://doi.org/10.1016/j.jnucmat.2022.153621.

Chalupová, A., Krejčí, J., Cvrček, L., Ševeček, M., Rozkošný, V., Přibyl, A., Halodová, P., Gávelová, P., 2019. Coated Cladding Behavior During High-temperature transients. APP 24. Doi: 10.14311/APP.2019.24.0009.

Csontos, A., Capps, N., 2019. Accident-Tolerant Fuel Valuation: Safety and Economic Benefits (Revision 1). EPRI.

Dunbar, C., Jung, W., Armstrong, R., Sridharan, K., Corradini, M., Yeom, H., 2024. Fuel performance analysis of Cr-coated Zircaloy-4 cladding during a prototypical LOCA event using BISON. Ann. Nucl. Energy 200, 110411. https://doi.org/10.1016/j.anucene.2024.110411.

European Commission, 2023. TRANSURANUS handbook (No. V1M1J23). Joint Research Centre.

Feria, F., Aragón, P., Herranz, L.E., 2024. Assessment of cladding ballooning during DBA-LOCAs with FRAPTRAN. Ann. Nucl. Energy 195, 110194. https://doi.org/10.1016/j.anucene.2023.110194.

Frederick, K., 2023. Accident Tolerant Fuel: Cr Coated Cladding Development at Westinghouse. Presented at the 28th International QUENCH Workshop, Karlsruhe, Germany.

Gabriel, A., Hawkins, L., French, A., Li, Y., Hu, Z., He, L., Xiu, P., Nastasi, M., Garner, Frank.A., Shao, L., 2022. Effect of dpa rate on the temperature regime of void swelling in ion-irradiated pure chromium. J. Nucl. Mater. 561, 153519. Doi: 10.1016/j.jnucmat.2022.153519.

Geelhood, K.G., Luscher, W.G., 2019. Degradation and Failure Phenomena of Accident Tolerant Fuel Concepts: Chromium Coated Zirconium Alloy Cladding (No. PNNL-28437 Revision 1). PNNL, Richland, Washington.

Geelhood, K., Luscher, W., Raynaud, P., Porter, I., 2014. FRAPCON-4.0: A Computer Code for the Calculation of Steady-State, Thermal-Mechanical Behavior of Oxide Fuel Rods for High Burnup (No. PNNL-19418, Vol.1 Rev.2). PNNL, Richland, Washington.

Geelhood, K., Luscher, W., Cuta, J., Porter, I., 2016. FRAPTRAN-2.0: A Computer Code for the Transient Analysis of Oxide Fuel Rods (No. PNNL-19400, Vol.1 Rev2). PNNL, Richland, Washington.

Guo, Z., Dailey, R., Zhou, Y., Sun, Z., Wang, J., Corradini, M.L., 2021. Effect of ATF Cr-coated-zircaloy on BWR In-vessel accident progression during a station blackout. Nucl. Eng. Des. 372, 110979. https://doi.org/10.1016/j.nucengdes.2020.110979.

Hagrman, D.L., 1981. Zircaloy Cladding Shape at Failure (BALON2) (No. EGG-CDAP-5379). Idaho National Engineering Laboratory.

Hazan, J., Gauthier, A., Pouillier, E., Shirvan, K., 2021. Semi-integral LOCA test of cold-spray chromium coated zircaloy-4 accident tolerant fuel cladding. J. Nucl. Mater. 550, 152940. https://doi.org/10.1016/j.jnucmat.2021.152940.

Holzwarth, U., Stamm, H., 2002. Mechanical and thermomechanical properties of commercially pure chromium and chromium alloys. J. Nucl. Mater. 300, 161–177. https://doi.org/10.1016/S0022-3115(01)00745-0.

IAEA, 2019. Fuel modelling in accident conditions (FUMAC): Final report of a Coordinated Research Project, IAEA-TECDOC-1889. IAEA, Vienna.

Kane, K., Bell, S., Capps, N., Garrison, B., Shapovalov, K., Jacobsen, G., Deck, C., Graening, T., Koyanagi, T., Massey, C., 2023. The response of accident tolerant fuel

cladding to LOCA burst testing: a comparative study of leading concepts. J. Nucl. Mater. 574, 154152. https://doi.org/10.1016/j.jnucmat.2022.154152.
Kim, H.-G., Kim, I.-H., Jung, Y.-I., Park, D.-J., Park, J.-Y., Koo, Y.-H., 2015. Adhesion property and high-temperature oxidation behavior of Cr-coated Zircaloy-4 cladding tube prepared by 3D laser coating. J. Nucl. Mater. 465, 531–539. https://doi.org/10.1016/j.jnucmat.2015.06.030.
Lahoda, E., Oelrich, R., Karoutas, Z., Ray, S., Boylan, S., Xu, P., Romero, J., Shah, H., 2018. Overview of Westinghouse Lead Accident Tolerant Fuel Program, in: Proceedings of the TopFuel 2018 Conference. Presented at the TopFuel 2018, Prague, Czech Republic.
Latu-Romain, L., Parsa, Y., Wouters, Y., 2019. Spallation study of chromia scales thermally grown on pure chromium in synthetic air. Mater. Charact. 152, 58–66. https://doi.org/10.1016/j.matchar.2019.04.011.
Lavoil, A., 2010. LOCA testing at Halden: The tenth experiment IFA-650.10 (No. HWR-974), OECD Halden reactor project. Institutt for energiteknikk, Halden, Norway.
Lee, Y., Yook, H., Kim, D., Joung, S., 2023. Exploring safety limits of Cr-coated ATF cladding using separate effect and integral LOCA experiments. Presented at the 28th International QUENCH Workshop, Karlsruhe, Germany. Doi: 10.5445/IR/1000165938.
Lee, Y., Lee, J.I., No, H.C., 2017. Mechanical analysis of surface-coated zircaloy cladding. Nucl. Eng. Technol. 49, 1031–1043. https://doi.org/10.1016/j.net.2017.03.012.
Lee, D.-Y., Ro, T.-S., Chung, B.-D., Hong, S.-J., 2023a. Implementation of chrome oxidation model into best-estimate system code for accident tolerant fuel. Ann. Nucl. Energy 192, 110002. https://doi.org/10.1016/j.anucene.2023.110002.
Luscher, W.G., Geelhood, K.J., Porter, I.E., 2015. Material Property Correlations: Comparisons between FRAPCON-4.0, FRAPTRAN-2.0, and MATPRO (No. PNNL-19417 Rev. 2). PNNL, Richland, Washington.
Ma, Z., Shirvan, K., Wu, Y., Su, G.H., 2021. Numerical investigation of ballooning and burst for chromium coated zircaloy cladding. Nucl. Eng. Des. 383, 111420. https://doi.org/10.1016/j.nucengdes.2021.111420.
Markiewicz, M.E., Erbacher, F.J., 1988. Experiments on Ballooning in Pressurized and Transiently Heated Zircaloy-4 Tubes (No. KfK 4343). Kernforschungszentrum Karlsruhe, Karlsruhe.
Mulligan, P.L., Nelson, A.T., Parish, C.M., Champlin, P.A., Chen, X., Morrall, D., Harp, J. M., 2024. Irradiation creep measurement and microstructural analysis of chromium nitride–coated zirconium alloy using pressurized tubes. J. Nucl. Mater. 588, 154808. https://doi.org/10.1016/j.jnucmat.2023.154808.
NEA, 2018. State-of-the-Art Report on Light Water Reactor Accident-Tolerant Fuels, Nuclear Science. OECD. Doi: 10.1787/9789264308343-en.
Neitzel, H.J., Rosinger, H.E., 1980. The Development of a Burst Criterion for Zircaloy Fuel Cladding under LOCA Conditions (No. KfK 2893). Kernforschungszentrum Karlsruhe, Karlsruhe, Germany.
Pouillier, E., 2023. e-ATF bibliographic survey on Chromium coated Zr-based materials (No. REP5.3.8), H2020 project R2CA WP5 INNOV.
Ridley, M., Bell, S., Garrison, B., Graening, T., Capps, N., Su, Y.-F., Mouche, P., Johnston, B., Kane, K., 2023a. Effects of Cr/Zircaloy-4 coating qualities for enhanced accident tolerant fuel cladding. Ann. Nucl. Energy 188, 109799. https://doi.org/10.1016/j.anucene.2023.109799.
Ridley, M., Massey, C., Bell, S., Capps, N., 2023b. High temperature creep model development using in-situ 3-D DIC techniques during a simulated LOCA transient. Ann. Nucl. Energy 193, 110012. https://doi.org/10.1016/j.anucene.2023.110012.
Ševeček, M., Chalupová, A., Čech, J., Walters, J., Maier, B., 2021. Experimental Evaluation of Chromium Cold-spray Coated Cladding. Presented at the TopFuel, Santander, Spain.
Ševeček, M., Gurgen, A., Seshadri, A., Che, Y., Wagih, M., Phillips, B., Champagne, V., Shirvan, K., 2018. Development of Cr cold spray–coated fuel cladding with enhanced accident tolerance. Nucl. Eng. Technol. 50, 229–236. https://doi.org/10.1016/j.net.2017.12.011.
Shackelford, J.F., Alexander, W., 2001. Materials Science and Engineering Handbook, 3rd ed. CRC Press LLC.
Simmons, G., Wang, H., 1971. Single Crystal Elastic Constants and Calculated Aggregate Properties. The MIT Press.
Stephens, J.R., Klopp, W.D., 1972. High-temperature creep of polycrystalline chromium (No. NASA TM X-2499). NASA, Washington.
Stuckert, J., Rössger, C., Walter, M., Große, M., Steinbrück, M., 2012. Results of the reference bundle test QUENCH-L1 with Zircaloy-4 claddings and future planning of the QUENCH-LOCA program.
Stuckert, J., Große, M., Rössger, C., Steinbrück, M., Walter, M., 2018. Results of the LOCA reference bundle test QUENCH-L1 with Zircaloy-4 claddings (No. SR-7651). KIT. Doi: 10.5445/IR/1000083067.
Sweet, R., Mouche, P., Bell, S., Kane, K., Capps, N., 2022. Chromium-coated cladding analysis under simulated LOCA burst conditions. Ann. Nucl. Energy 176, 109275. https://doi.org/10.1016/j.anucene.2022.109275.
USNRC, 2020. Supplemental Guidance Regarding the Chromium-Coated Zirconium Alloy Fuel Cladding Accident Tolerant Fuel Concept (No. ATF-ISG-2020-01). USNRC.
Vidal, J.M., Río, I., Walters, J., Long, Y., Linsuain, O., 2022. Out-Of-Reactor Creep Analysis of Chromium Surface-Coated Optimized ZIRLO™ Cladding, in: TopFuel 2022 Light Water Reactor Fuel Performance Conference. Presented at the TopFuel 2022 Light Water Reactor Fuel Performance Conference, American Nuclear Society, Raleigh, NC, pp. 326–333. Doi: 10.13182/TopFuel22-38932.
Wagih, M., Spencer, B., Hales, J., Shirvan, K., 2018. Fuel performance of chromium-coated zirconium alloy and silicon carbide accident tolerant fuel claddings. Ann. Nucl. Energy 120, 304–318. https://doi.org/10.1016/j.anucene.2018.06.001.
Walters, J.L., Romero, J.E., Mueller, A.J., Maier, B.R., Partezana, J.M., Lyons, J.L., Byers, W.A., Wang, G., Parsi, A., Stiteler, R.S., Limback, M., 2021. Effects of Cold Spray Chromium Coatings on the Properties of Zirconium Alloys. Presented at the Zirconium in the Nuclear Industry: 19th International Symposium, West Conshohocken, PA, pp. 211–231. Doi: 10.1520/STP162220190065.
Yang, J., Steinbrück, M., Tang, C., Große, M., Liu, J., Zhang, J., Yun, D., Wang, S., 2022. Review on chromium coated zirconium alloy accident tolerant fuel cladding. J. Alloy. Compd. 895, 162450. https://doi.org/10.1016/j.jallcom.2021.162450.